Available online at www.sciencedirect.com
ScienceDirect
International Journal of Heat and Mass Transfer 50 (2007) 3437–3446
International Journal of HEAT and MASS TRANSFER
www.elsevier.com/locate/ijhmt

A generalized mathematical description for comparative assessment of various horizontal polar tube geometries with regard to external film condensation in presence of non-condensable gases

Saumyadip Mukhopadhyay, S.K. Som, Suman Chakraborty *

Department of Mechanical Engineering, Indian Institute of Technology, Kharagpur 721302, India

Received 9 June 2006; received in revised form 29 December 2006
Available online 30 March 2007

Abstract

A generalized mathematical treatment is postulated to investigate the condensation heat transfer performance of horizontal tubes with varying geometries, with the presence of non-condensable gases in the free stream. The governing equations of mass, momentum and energy conservation in the liquid phase are solved semi-analytically, with matching constraints being imposed at the liquid–vapour interface, while the governing equations of energy and species conservation in the vapour phase are solved numerically. An air–water vapour system is considered for demonstrating the mathematical model. Special cases of the model are illustrated with the aid of elliptical and equiangular spiral geometries. It is revealed that the geometrical features of typical polar surfaces can turn out to be favourable in arresting probable drastic reductions in the condensation heat transfer rates that could be otherwise associated with the presence of non-condensable gases in the free stream. The favourable effects induced by polar surfaces become relatively more prominent, as percentage of non-condensable gases in the free stream increases. A geometrical shape function is also ascertained in this regard, which quantifies the extent of this augmentation in the heat transfer performance. In general, it is suggested that polar surfaces with higher values of the shape function over a majority of the azimuthal regime can turn out to be more desired choices for achieving enhanced rates of condensation heat transfer, provided that there are no serious manufacturability constraints.

Keywords: Film condensation; Non-condensable; Diffusion; Polar surfaces; Horizontal tubes

1. Introduction

Film condensation of vapours has been extensively studied by the research community during the last century [1–12], primarily motivated by its relevance in the design of heat exchangers in the chemical processing units and power industries. Starting from the fundamental study of Nusselt [1], several other authors [2–25] have reported significant contributions towards the understanding of heat and mass transfer mechanisms associated with film condensation on external surfaces. With a further motivation of designing compact and yet more effective heat exchangers, a significant effort has subsequently been devoted to enhance the film-wise condensation rates on horizontal condensing tubes. The earlier efforts in this regard have been directed towards the employment of passive heat enhancement techniques, such as the introduction of extended surfaces, as potential enhancers of the surface area to volume ratio, in conjunction with the utilization of the surface tension effects to obtain thinner condensate films. Alternatively, researchers have also proposed non-circular geometries [3–12], which might offer with a natural provision of thinning the condensate film deposition, by directly exploiting the effects of surface tension, as manifested through the establishment of strong pressure gradients in the stream wise direction (i.e., along the surface profile), and a simultaneous aiding effect of gravity as a consequence of placement of a larger proportion of the condensing surface in

* Corresponding author. Tel.: +91 3222282990; fax: +91 3222282278.
E-mail address: suman@mech.iitkgp.ernet.in (S. Chakraborty).

0017-9310/$ - see front matter © 2007 Elsevier Ltd. All rights reserved.
doi:10.1016/j.ijheatmasstransfer.2007.01.042

Nomenclature

a	geometric surface parameter
b	semi-minor axis of the ellipse
C	concentration
C_p	specific heat of condensate at mean film temperature
D_e	equivalent diameter of a circular tube with the same condensing surface area
e	eccentricity of the ellipse, $\frac{\sqrt{a^2-b^2}}{a}$
$F(\theta)$	polar function describing the velocity profile
g	acceleration due to gravity
h	local heat transfer coefficient
$\bar{h}$	average heat transfer coefficient
h_{fg}	latent heat due to condensation
Ja	Jacob number, $\frac{C_p\left(T_{sat,i}-T_w\right)}{h_{fg}\vert_{T=T_{sat,i}}}$
K	thermal conductivity of the species
L	length of semi perimeter of any polar curve
M	molar mass
$\dot{m}$	mass flow rate of cooling liquid flowing through the tube
$\dot{m}_c$	mass flux of condensate
N_σ	non-dimensional surface tension force, $\frac{4\sigma}{(\rho_l-\rho_v)gD_e^2}$
Nu	local Nusselt number, $\frac{hD_e}{K_l}$
$\overline{Nu}$	average Nusselt number
p_σ	pressure due to surface tension
R	polar radius of a point on the condenser profile
R_c	radius of curvature
Ra	Rayleigh number, $\frac{\rho_l(\rho_l-\rho_v)gD_e^3C_p}{\mu_lK_l}$
r	radial coordinate of any point in the flow domain
T	temperature
T_c	critical temperature of water
v	velocity

Greek symbols

β	angle between the tangent to the polar surface and the direction of action of gravity, at any point on tube surface
δ	liquid film thickness
θ	polar angle of any point, as measured from the vertical
μ	dynamic viscosity
ρ	density
σ	surface tension coefficient
ϕ	parametric angle of any point on the tube surface

Subscripts

a	reference condition
c	circular
g	gas, non-condensible
i	interface
l	liquid phase
p	polar
r	radial direction
sat	saturation
v	vapour phase
w	wall
x_1	stream-wise direction along the tube surface
y_1	cross stream-wise direction at any point to the tube surface
∞	free stream

line with the vertical. In particular, elliptic tubes with different eccentricities [4–11] have been extensively investigated with an intention of obtaining augmented rates of the overall heat transfer. The first comprehensive analysis on laminar film condensation of saturated vapour on inclined elliptical tubes considering surface tension effects has been carried out and reported by Fieg [6]. Dutta et al. [12], in a more recent study, have explored the advantages associated with the employment of condensing tube surfaces in the form of equiangular spirals, in order to achieve enhanced rates of heat transfer.

Although, most of the above-mentioned investigations have been concerned with the condensation of pure saturated vapours, a small amount of non-condensable gas is expected to be invariably present in any practical condensing system, as a consequence of leakages prevailing in the same, or due to a dissolution of the condensing vapour. In this regard, it has been well established that the existence of non-condensable gases in the system can greatly reduce the condensation heat transfer rates and significantly deteriorate the performance of the condensers, primarily by the virtue of the fact that non-condensable gas boundary layer formed at the liquid–vapour interface serves as an additional resistance against the vapour condensation to take place. Minkowycz and Sparrow [15] executed a pioneering investigation to analyse the effects of interfacial resistance, superheat in the vapour, thermo-solutal buoyancy driven convection and the property variations on the condensation heat transfer in presence of non-condensable vapours. Subsequent investigations on this topic have been executed by several other authors in the past few decades [17–25]. Of particular interest has been the condensation heat transfer on external surfaces, in presence of non-condensables in the free stream, mainly because of its technological relevance. Although, a number of research publications on this central theme exist in the literature, a generalized mathematical treatment for analyzing film condensation over surfaces with disparate geometrical attributes is yet to be reported. In practice, however, such kinds of generalization could be immensely critical in providing a common basis for comparing the heat transfer performance of condensing tube surfaces of varying geometries, in presence of non-

condensable gases, in an effort to arrive at an optimized design of the heat exchanging surface contour.

Aim of the present work is to establish a generalized mathematical formalism for analyzing external condensation heat transfer over surfaces with varying geometrical shapes, in the presence of non-condensables in the free stream. This is systematically achieved by obtaining the evolution of the condensing film thickness as a function of the generalized polar angle, from a coupled solution of mass, momentum and energy conservation equations, with matching interfacial constraints. In order to obtain a generalization in the condensation behaviour in the presence of non-condensables, separate treatments of the liquid and the vapour phases have been introduced. Based on the generalized theoretical proposition developed in this study, a direct comparison of the tube geometries of various polar forms can be possible, so as to quantitatively asses the capabilities of their geometrical features to arrest an otherwise drastic reduction in the heat transfer rates due to the influence of non-condensable gases. As an illustration, tube surfaces of circular, elliptic and equiangular polar shapes are compared, in an effort to pinpoint their relative performance in achieving a desired rate of heat transfer, despite the adverse effects imposed by the presence of non-condensable gases in the free stream.

2. Mathematical modeling

Fig. 1 is the schematic representation of a generic condensing surface, with 'x_1' as the generalized stream-wise coordinate and 'y_1' as the corresponding cross-stream wise coordinate. In terms of polar coordinates, the surface is described as $R(\theta)$, where θ is the angle between the vertical and the radial direction at any point on the condensing surface contour. As the condensing vapour comes in contact with the external surface of the condenser, a thin condensate film can readily form adhering to the same, separating the tube surface from the bulk vapour stream. The mathematical model depicting the thermo-solutal transport in the condensate and the free stream can be formulated by appealing to the pertinent conservation equations of mass, momentum and thermal energy. In-built with the mathematical model presented here are certain major simplifying assumptions, as follows:

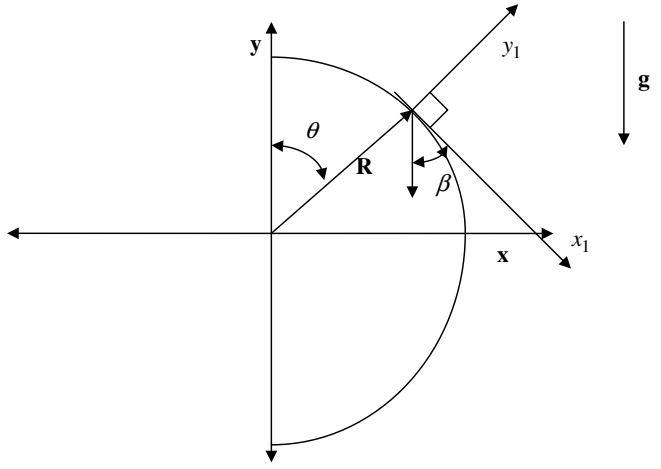

Fig. 1. A schematic diagram depicting the geometrical parameters associated with a condensing surface of an arbitrary geometry.

1. The condensed liquid film adhering to the tube surface is thin enough, so that temperature distribution within the same can assumed to be linear.
2. The flow Reynolds number in the condensate film is small enough so that the convective terms in the linear momentum conservation equation for the liquid phase can be neglected.
3. Fluid flow is incompressible and laminar.
4. Local thermodynamic equilibrium prevails at the liquid vapour interface.
5. The condensing tube surface is isothermal ($T = T_w$).
6. Vapour phase is otherwise stagnant except having only radial flow velocity due to mass diffusion.
7. Film surface and wall surface have the same radius of curvature $R_c(\theta)$ at all angular locations.
8. Viscosity of the condensate is taken to be temperature-independent.

One may begin with the analysis by first noting that the governing equation for linear momentum conservation in the liquid phase can be written as

$$\mu_l \frac{d^2 v_{x_1}}{dy_1^2} = -(\rho - \rho_v) g \cos\beta + \frac{dp_\sigma}{dx_1} \tag{1}$$

where β denotes the angle between gravity and tangent to any point on the surface (refer to Fig. 1) and $\frac{dp_\sigma}{dx_1}$ denotes the pressure gradient due to surface tension. The p_σ term can be accounted for by a balance of surface tension and pressure forces at the interface as

$$p_\sigma = \frac{\sigma}{R_c} \tag{2}$$

where σ is the surface tension coefficient and R_c is the local radius of curvature, which, in general, can be defined as

$$R_c = \frac{(R^2 + R'^2)^{\frac{3}{2}}}{(R^2 + 2R'^2 - RR'')} \tag{3}$$

where '$'$' denotes differentiation with respect to θ. Based on Eq. (3), one may obtain an expression for $\frac{dp_\sigma}{dx_1}$ for a generalized polar surface, as

$$\frac{dp_\sigma}{dx_1} = -\left(\frac{\sigma}{R_c^2}\right)\left(\frac{dR_c}{d\theta}\right)\left(\frac{d\theta}{dx_1}\right) \tag{4}$$

where,

$$dx_1 = \sqrt{dR^2 + (Rd\theta)^2} \tag{4a}$$

Eq. (1) can be analytically solved with the aid of the following boundary conditions: $v_{x_1} = 0$ at $y_1 = 0$ and $\frac{dv_{x_1}}{dy_1} =$

0 at $y_1 = \delta$, where δ is the condensate film thickness. This leads to the following velocity profile in the liquid film

$$v_{x_1} = \frac{(\rho - \rho_v)g}{\mu_l} y_1 \left(\delta - \frac{y_1}{2}\right) F(\theta) \tag{5}$$

where,

$$F(\theta) = \left(\frac{\mathrm{d}p_\sigma/\mathrm{d}x_1}{(\rho_l - \rho_v)g} + \cos\beta\right) \tag{5a}$$

It is important to note here that the function $F(\theta)$ represents the sole influence of the geometrical characteristics of the surface on the liquid phase velocity profile. An important aim of the subsequent analysis, therefore, would be to investigate the influence of this function on the condensation heat transfer performance of various tube geometries.

Analysis for the flow-field in the vapour phase can be carried out by first referring to the continuity equation in the following form:

$$\frac{1}{r}\frac{\partial}{\partial r}(r v_r) + \frac{1}{r}\frac{\partial}{\partial \theta}(v_\theta) = 0 \tag{6}$$

Since the characteristic cross-radial component of velocity is much smaller than the characteristic radial component of velocity (which is the Stefan flow velocity) and the characteristic length scale along the tube surface profile is larger than that along the radial direction, it can be inferred that the first term in the left hand side of Eq. (6) dominates over the second term in an order of magnitude sense. Hence, it can be inferred that

$$v_r \propto \frac{1}{r} \tag{6a}$$

Now, assuming $v_r = v_s(\theta)$ at $r = R + \delta$ (liquid–vapour interface) and $\delta \ll R$, Eq. (6a) leads to the following expression for v_r in terms of v_s (θ)

$$v_r = \frac{v_s(\theta) R}{r}. \tag{7}$$

In Eq. (7), v_s (θ) is the radial velocity at the liquid–vapour interface, which can be determined from the conditions of impermeability of the interface to the non-condensing species. Using Eq. (7), the energy and species conservation equations in the vapour phase can be expressed in the following simplified forms:

$$\left(\frac{v_s(\theta)R}{r}\right)\frac{\partial T_v}{\partial r} = \alpha_v\left(\left(\frac{\partial^2 T_v}{\partial r^2}\right) + \frac{1}{r}\left(\frac{\partial T_v}{\partial r}\right) + \frac{1}{r^2}\left(\frac{\partial^2 T_v}{\partial \theta^2}\right)\right) \tag{8}$$

$$\left(\frac{v_s(\theta)R}{r}\right)\frac{\partial C_v}{\partial r} = D\left(\left(\frac{\partial^2 C_v}{\partial r^2}\right) + \frac{1}{r}\left(\frac{\partial C_v}{\partial r}\right) + \frac{1}{r^2}\left(\frac{\partial^2 C_v}{\partial \theta^2}\right)\right) \tag{9}$$

where the subscript 'v' refers to vapour phase, T is the temperature, C is the concentration of the condensable phase, α is the thermal diffusivity and D is the mass diffusion coefficient. The boundary conditions consistent with Eqs. (8) and (9) are as follows:

$$\text{At } r = R T_v = T_i,\ C_v = C_i, \tag{10a}$$

where the subscript 'i' refers to the conditions at liquid–vapour interface.

$$\text{At } r \to \infty \text{ (taken to be } 10R \text{ for the numerical computations)},\ T_v = T_\infty,\ C_v = C_\infty, \tag{10b}$$

where T_∞ is the saturation temperature corresponding to a mass fraction of C_∞ of the condensable in the vapour phase.

$$\text{At } \theta = \tan^{-1} m \text{ and } \theta = \pi, \quad \frac{\partial T_v}{\partial \theta} = 0, \quad \frac{\partial C_v}{\partial \theta} = 0 \tag{10c}$$

It is noteworthy to mention here that the interfacial vapour temperature and concentration values are thermodynamically inter-linked from local equilibrium considerations, as per which the interfacial temperature is nothing but the saturation temperature of the vapour at its partial pressure at the interface, which in turn depends on the concentration of the vapour at the interface. In the present investigation, water is assumed to be the condensing phase and air is taken to be the non-condensable gaseous phase. For such air–water vapour systems, the partial pressure of the vapour at the interface can be expressed as a unique function of interfacial saturation temperature as follows [23]:

$$\frac{p_v}{p_{total}} = \exp\left[\frac{h_{fg,a}}{R}\left\{\frac{T_i - T_a}{T_i T_a}\right\} - \frac{0.38}{T_c}\ln\frac{T_i}{T_a} - \frac{0.118}{T_c^2}\{T_i - T_a\}\right] \tag{11}$$

where $h_{fg,a}$ is the latent heat of condensation of steam at a reference temperature T_a, T_c is the critical temperature of water and p_{total} is the total pressure of the mixture. The interfacial mass fraction of the vapour can be expressed as

$$C_i = \frac{1}{1 + \frac{M_{air}}{M_{water}}\left(\frac{p_{total}}{p_v} - 1\right)} \tag{12}$$

where M denotes the molar mass of the corresponding species. The radial velocity at the liquid–vapour interface, as appearing in Eqs. (8) and (9), can be expressed as

$$v_s = -D\frac{\left(\frac{\partial C_v}{\partial y_1}\right)_{y_1=\delta}}{(1 - C_v)_i} \tag{13}$$

A physical basis of Eq. (13) can be provided as follows. The non-condensable gas is transported from the bulk vapour phase to the interface by the same advective flow that also carries the condensable phase. However, impermeability constraints of the non-condensable gas at the interface drive off the non-condensable phases from the interface to the bulk by means of diffusive transport, at the same rate at which it is transported into the interface. This, in turn, physically implies that an adequately high value of the non-condensable concentration is expected to build up at the liquid–vapour interface, so as to counterweigh an incoming convective transport with a strong gradient-driven back-diffusional transport of the non-condensable species.

It is also important to mention here that the liquid and the vapour phase temperature distributions are implicitly interlinked with the Stefan balance condition at their interface, which necessitates

$$\dot{m}_c h_{fg} = K_l(\partial T_l/\partial y_l)_{y_l=\delta} - K_v(\partial T_v/\partial y_l)_{y_l=\delta} \tag{14}$$

where $\dot{m}_c$ is the rate of condensation mass transfer and K is the thermal conductivity. Because of the assumption of a linear temperature profile in the liquid phase, the term $(\partial T_l/\partial y_l)_{y_l=\delta}$ in Eq. (14) reduces to $\left(\frac{(T_i-T_w)}{\delta}\right)$. Further, $\dot{m}_c$ can be calculated explicitly from the liquid phase velocity profile, by noting that the difference in the mass flow rates across the two opposite faces of an infinitesimally small liquid control volume (coaxial with the x_l direction) is accounted for by the condensation of the overlying vapour phase to form the condensate phase. This can be mathematically described as

$$\dot{m}_c = \frac{d}{dx_l}\left(\int_0^\delta \rho_l v_{x_l} dy_l\right) \tag{15}$$

Combining Eqs. (14) and (15) with the velocity profile given by Eq. (5), the following ordinary differential equation can be obtained:

$$\frac{d(\delta^3 F(\theta))}{dx_l} = \left(\frac{3\mu_l K_l(T_i - T_w)}{h_{fg}\rho_l(\rho_l-\rho_v)g}\right)\frac{1}{\delta} - \left(\frac{3\mu_l K_v}{h_{fg}\rho_l(\rho_l-\rho_v)g}\right)\left(\frac{\partial T_v}{\partial y_l}\right)_{y_l=\delta}, \tag{16}$$

which can be further simplified to the following form

$$\frac{d(\chi)}{d\theta} = \left(\left(\frac{3\mu_l K_l(T_i - T_w)}{h_{fg}\rho_l(\rho_l-\rho_v)g}\right)\frac{F(\theta)^{1/3}}{\chi^{1/3}} - \left(\frac{3\mu_l K_v}{h_{fg}\rho_l(\rho_l-\rho_v)g}\right)\left(\frac{\partial T_v}{\partial y_l}\right)_{y_l=\delta}\right)\left(\frac{dx_l}{d\theta}\right) \tag{16a}$$

where $\chi = \delta^3 F(\theta)$ and $F(\theta)$ is given by Eq. (5a).

In practice, a solution to Eq. (16a) is obtained as follows. First, a coupled numerical solution of the vapour phase temperature and concentration profiles is obtained by employing a control volume based finite difference method. The resultant solution of the vapour phase temperature field is substituted in Eq. (16a), which is then solved by employing a fourth order Runge–Kutta method, to obtain the thickness of the condensate phase as a function of the polar angle. Based on this information, the overall convective heat transfer coefficient, h, is calculated as follows

$$h = \frac{K_l(T_i - T_w)}{\delta(T_\infty - T_w)} \tag{17}$$

The Nusselt number, Nu, is defined as

$$Nu = \frac{hD_e}{K_l} = \frac{D_e(T_i - T_w)}{\delta(T_\infty - T_w)} \tag{18}$$

where D_e is the diameter of an equivalent circular cylinder that has the same external surface area as that of the given surface under consideration. The concept of such an equivalent diameter [6] has been introduced in the analysis to offer ready comparison bases for condensation performance of tubes with varying surface contours, with all other conditions remaining unaltered. The area-averaged Nusselt number can be calculated as

$$\overline{Nu} = \frac{\int NuR\sqrt{1+\left[\frac{d}{d\theta}(\ln R)\right]^2}d\theta}{\int R\sqrt{1+\left[\frac{d}{d\theta}(\ln R)\right]^2}d\theta}, \tag{19}$$

which is nothing but a non-dimensionalized representation of the average heat transfer coefficient over the condenser tube surface, R being the local polar radius of the profile corresponding to an angle θ. The mathematical descriptions presented through Eqs. (1)–(19) are fairly general and are independent of any specific choice of the condensing surface profile. However, it can readily be observed that the function $F(\theta)$ appears as a distinctive influencing parameter that varies from one surface profile to another and effectively inculcates the details of the geometric features of tube surface that are responsible for draining the condensate film, attributed to a combined effect of the surface-tension driven pressure gradient and the gravity force component acting in the streamwise direction. Because of this critical significance, we term $F(\theta)$ as the condensing surface shape function, since it alone dictates the influence of the shape of the condensing surface on the overall condensation performance. Table 1 illustrates the exact mathematical forms of this function, along with other auxiliary geometry-dependent parameters, corresponding to various surface forms, as obtained from the present generalized formulation. It can easily be observed from the table that a wide variety of shapes, ranging from circular, elliptic to equiangular spiral profiles, can all be analyzed by the unified sets of model expressions developed in this study. The different tube profiles considered in the present study are as follows:

(i) An equiangular spiral (Fig. 2a): in this geometry, the entire symmetrical half of the polar curve cannot be taken to model the tube surface, since there exists an upward sloping portion, bounded by, $0 \leqslant \theta \leqslant \tan^{-1} m$ in which the condensate cannot flow with the aid of gravity. This leads to the consideration of a surface formed by the segment of the polar profile $R = ae^{m\theta}$, described on a vertical chord BE, as shown in the figure. The segment BGE represents the half of the tube surface, with chord BE as the axis of symmetry. It can be noted here that for this geometry, the term $\sqrt{1+\left[\frac{d}{d\theta}(\ln R)\right]^2}$ becomes a constant ($\sqrt{1+m^2}$), so that one may also evaluate the area-averaged Nusselt number by employing the following simplified expression: $\overline{Nu} = \frac{\int NuRd\theta}{\int Rd\theta}$. This kind of sim-

Table 1
A summary of the geometry-dependant attributes for various surface forms, pertinent to their condensation performance

	Circle	Ellipse	Equiangular spiral
R	a	$a\sqrt{\dfrac{1-e^2}{1-(e\sin(\theta))^2}}$	$ae^{m\theta}$
R_c	a	$\dfrac{a^2}{b}\left(\dfrac{1+e^4\cos^2\theta-2e^2\cos^2\theta}{(1-(e\cos\theta)^2)}\right)^{3/2}$	$ae^{m\theta}\sqrt{(1+m^2)}$
$\left(\dfrac{dx_1}{d\theta}\right)$	a	$a\sqrt{1-e^2}\left(\dfrac{1+e^4\cos^2\theta-2e^2\cos^2\theta}{\left(1-(e\cos\theta)^2\right)^3}\right)^{1/2}$	$ae^{m\theta}\sqrt{(1+m^2)}$
$\dfrac{dp_\sigma}{dx_1}$	0	$\dfrac{3b}{2a^2}\dfrac{\sigma e^2\sin 2\phi}{(1-e^2\cos^2\phi)^{5/2}}\dfrac{\sqrt{1-(e\cos\theta^2)}}{a\sqrt{1-2e^2\cos^2\theta+e^4\cos^2\theta}}$	$\dfrac{\sigma m e^{-2m\theta}}{a^2(1+m^2)}$
β	$\pi/2-\theta$	$\dfrac{\pi}{2}-\tan^{-1}\left(\dfrac{\tan\theta}{1-e^2}\right)$	$\dfrac{\pi}{2}-\tan^{-1}m-\theta$
$F(\theta)$	$\sin\theta$	$\dfrac{3b}{2a^2}\dfrac{1}{(\rho_l-\rho_v)g}\dfrac{\sigma e^2\sin 2\phi}{(1-e^2\cos^2\phi)^{5/2}}\dfrac{\sqrt{1-(e\cos\theta^2)}}{a\sqrt{1-2e^2\cos^2\theta+e^4\cos^2\theta}}$ $+\cos\left(\dfrac{\pi}{2}-\tan^{-1}\left(\dfrac{\tan\theta}{1-e^2}\right)\right)$	$\dfrac{\sigma m e^{-2m\theta}}{(\rho_l-\rho_v)ga^2(1+m^2)}$ $-\cos\left(\dfrac{\pi}{2}+\tan^{-1}m+\theta\right)$
D_e	$2a$	$D_e=\frac{2a}{\pi}\int_0^\pi g(\phi)d\phi$ where, $g(\phi)=\left(\dfrac{(1-e^2)+\frac{e^4}{4}\sin^2 2\phi}{1-\frac{e^2}{4}\sin^2 2\phi}\right)$	$\dfrac{2a(1+m^2)^{\frac{1}{2}}}{\pi m}\times\left(e^{\left(\frac{\pi}{2}+\phi\right)m}-e^{m\tan^{-1}m}\right)$ where the angle ϕ is obtained from $\cos\phi=\dfrac{ae^{m\tan^{-1}m}\sin(\tan^{-1}m)}{ae^{m(\pi/2+\phi)}}$

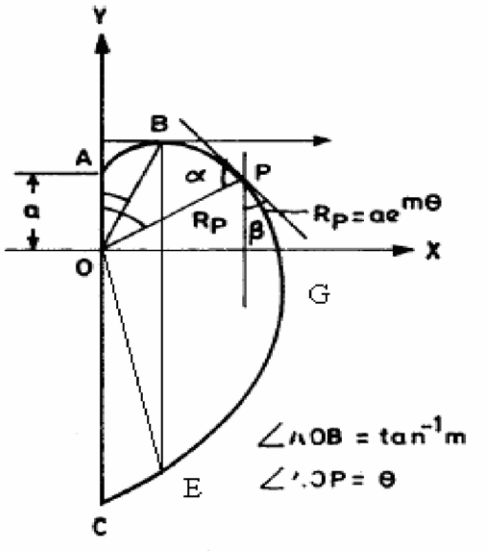

Fig. 2a. An equiangular spiral curve generated on the vertical axis.

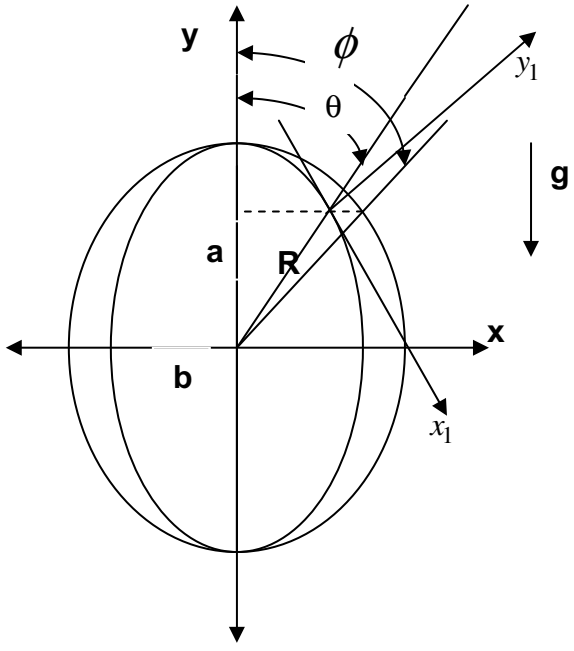

Fig. 2b. A horizontal ellipse with major axis aligned along gravity.

plification, however, is not possible in general for all other tube profiles (for example, for the case of an elliptically shaped tube profile), except for pure circular ones.

(ii) An ellipse (Fig. 2b): a horizontal elliptic tube with the major axis aligned with the direction of gravity.

(iii) A purely circular one (for the purpose of comparison).

These surfaces have been specifically chosen, because of the fact that several researchers have extensively studied the condensation heat transfer characteristics over tubes with such geometrical contours, in the recent past [2–12,23].

For the purpose of illustration, the variations of the function $\cos\beta$ with θ, for equiangular spiral and elliptic shapes are depicted in Figs. 3 and 4, respectively. It can be observed that for an equiangular spiral, higher values of the geometrical parameter m result in a consequent

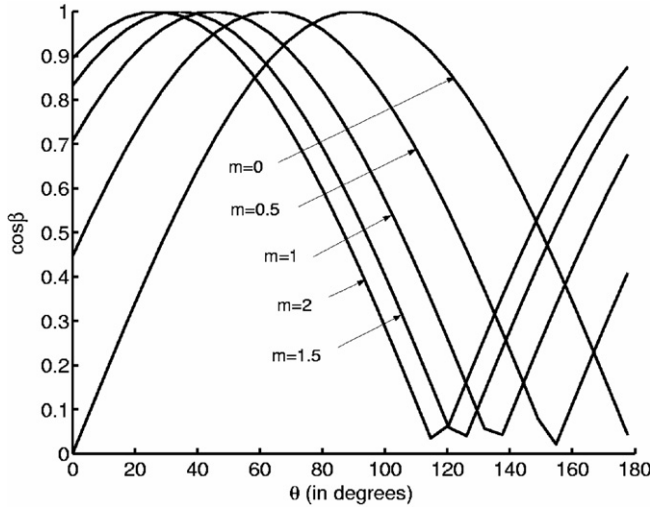

Fig. 3. Variations in the surface function $\cos\beta$ for an equiangular spiral geometry with variations in the polar angle, for different values of the polar constant.

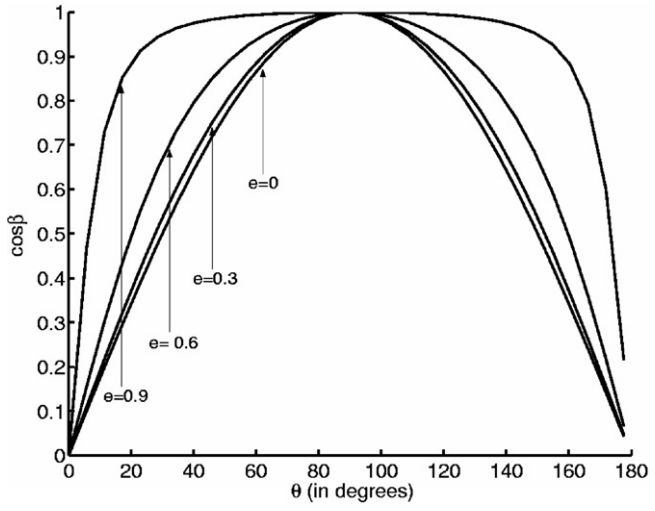

Fig. 4. Variations in the surface function, $\cos\beta$, for an elliptic geometry with the variations in the polar angle, for different values of the eccentricity.

phase lead in the $\cos\beta$ vs. θ characteristics. The function $F(\theta)$, in this case, is the sum of two independent contributions, namely, an explicit geometry-dependent component $\left(-\cos\left(\frac{\pi}{2}+\tan^{-1}\mathrm{m}+\theta\right)\right)$ and another component that depends on the relative influence of geometrical contributions to the net surface tension and gravity effects $\left(\frac{\sigma m e^{-2m\theta}}{(\rho_1-\rho_v)ga^2(1+m^2)}\right)$. The contribution of the later component towards the overall variations in $F(\theta)$ turns out to be rather inconsequential, which in turn implies that the gravity dependent component overweighs the surface tension dependent component to a significant extent. Fig. 4 depicts a very similar variation for the elliptical shapes. In general, it is observed that higher the eccentricity (e) of the ellipse, wider is the θ-domain over which a substantially high value of $\cos\beta$ is maintained. Analogous to the observation made in case of the equiangular spiral, the role of surface tension driven component is ascertained to be negligible in this case as well, as compared to the effects of gravity.

3. Results and discussion

One of the primary motivations behind this investigation is to obtain an effective comparison between the condensation performances of varying geometries, by utilizing a generalized mathematical framework. The physical parameters for which these cases are investigated can be translated in terms of two dimensionless groups [12], namely, $\left(\frac{Ra}{Ja}\right)^{\frac{1}{4}}$ and N_σ, where Ra is the Rayleigh number, Ja is the Jacob number and N_σ is a ratio depicting the relative importance of surface tension and the gravity effects for a specified equivalent diameter. Typical values of these parameters, as employed in the present study, are taken from Dutta et al. [12]. Values of the thermodynamic parameters are taken from Som and Chakraborty [23]. Under specified values of these physical parameters, selection of the geometrical characteristics pertinent to various surface profiles is critical to the performance of the condenser. However, the geometrical characteristics are also, in practice, restrained within the practical considerations of manufacturability of the desired shape. For example, a practical guideline of the ranges of eccentricity values for elliptically shaped condensing tubes, based on manufacturing constraints, has been reported to be $0 \leqslant e \leqslant 0.9$ (approximately) [9]. Analogous restraints have also been identified for equiangular spiral shapes, with $1 \leqslant m \leqslant 2$ [14]. Within these constraints, higher values of the parameters m (for equiangular spiral) and e (for ellipse) essentially imply higher values of the function $F(\theta)$ prevailing over a majority of the azimuthal range, leading to lower values of δ, and consequent enhancements in the rates of condensation heat transfer. Therefore, for an inter-comparison between these two shapes, upper limits of these parameters are chosen as m (polar constant for an equiangular spiral)=2 and e (eccentricity for an ellipse) 0.9 in this study.

Fig. 5 shows a variation of the non-dimensional liquid film thickness, $\delta^* = \delta\left(\frac{D_e K_1 \mu_1 (T_\infty - T_w)}{h_{fg}(\rho_1-\rho_v)\rho_1 g}\right)^{-1/4}$, over the tube surface of different geometries, for various values of free stream concentration of non-condensable gases. The figure depicts a gradual increase in film thickness, as one moves progressively along the streamwise direction, x_1. It is observed that the film thickness at any polar angle is higher with lower free stream concentrations of the non-condensable gas, for all the polar surfaces. An elucidation to this observation may be made from the dependence of film thickness on the temperature difference, $(T_i - T_w)$, as depicted in the Nusselt's classical theory on film condensation over a vertical flat plate in presence of non-condensable species [14]. The interfacial temperature, T_i, equals to the saturation temperature corresponding to partial pressure of vapour at the interface. The vapour pressure at interface, again, depends on the local concentration of non-condensable species which is being controlled by its

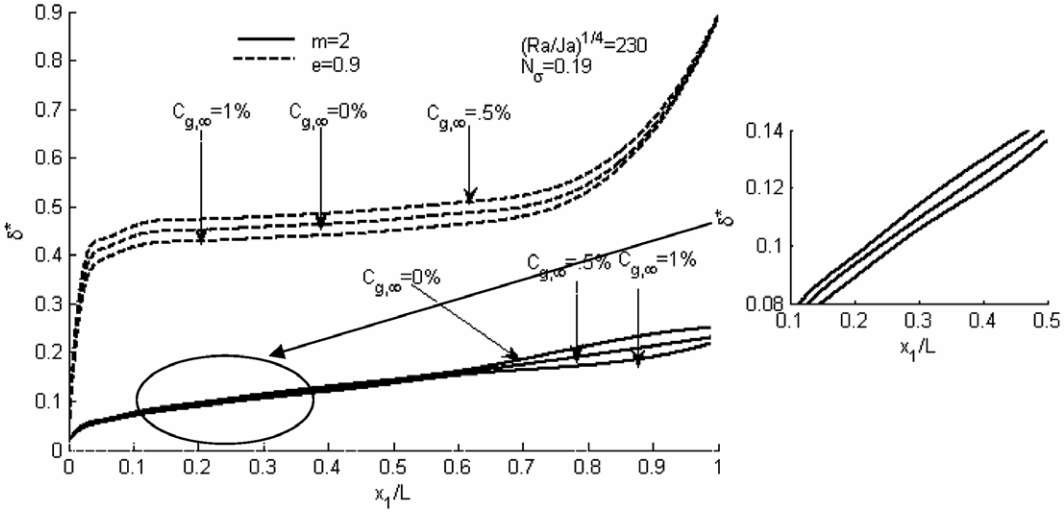

Fig. 5. Non-dimensional film thickness as a function of the non-dimensional streamwise coordinate, for different values of free stream concentrations of the non-condensables. Condensing surfaces with equiangular spiral ($m = 2$) and elliptical shapes ($e = 0.9$) are considered to generate these plots.

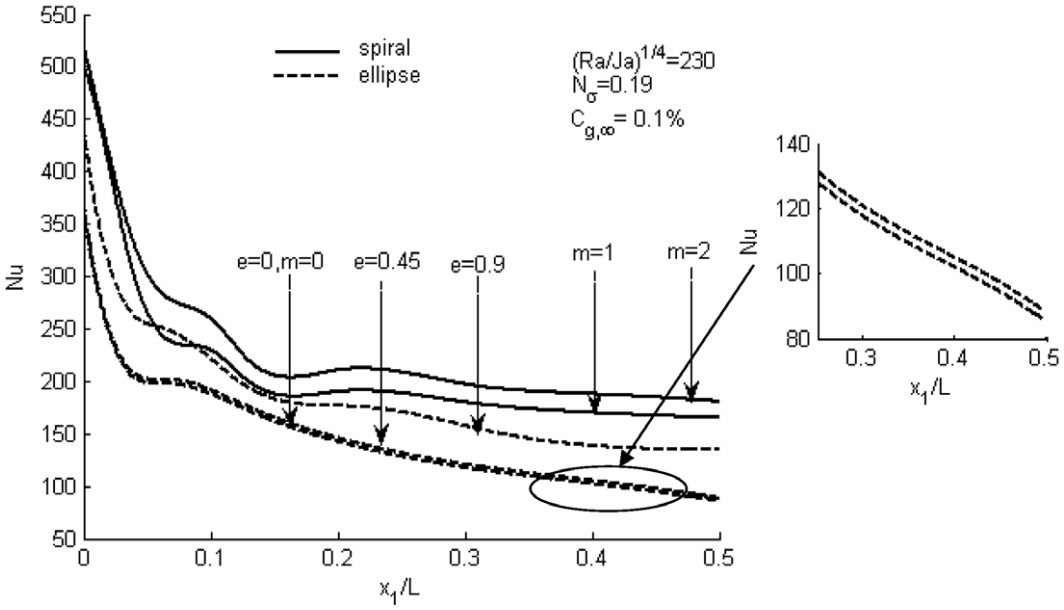

Fig. 6. Variation in the local Nusselt number along the tube periphery, for condensing surfaces with equiangular spiral and elliptical shapes.

diffusive flow from the interface to the bulk. Hence, a decrease in the free stream concentration of the non-condensable gas results in a lower concentration build up of the same at the interface, thereby increasing the value of $(T_i - T_w)$, consequently leading to an increase in the condensate film thickness.

The comparison between non-dimensional film thicknesses for various surface geometries is the highlight of Fig. 5. It is observed that the film thickness for an equiangular spiral is lower than that for an ellipse with the same condensing surface area. This can be explained on the basis of some observations from the plots of $\cos\beta$ vs. θ (Figs. 3 and 4). The function $F(\theta)$ implies the components of the surface tension driven pressure gradient and gravity in the direction of condensate flow. It can be noticed that for $m = 2$, the values attained by $F(\theta)$ are initially quite high, as compared to those obtained in case of an ellipse of eccentricity $e = 0.9$, thereby driving the condensate much faster, resulting in a decrease in the film thickness. A mathematical approach to explain this phenomenon can be obtained by a cognitive consideration of the fact that the growth of film thickness is directly proportional to the term $\left(\frac{dx_1}{d\theta}\right)$, the order of which is equivalent to that of the geometric parameter 'a' (Table 1). It can be easily established from geometric considerations that for a specified value of 'a', the surface area for a spiral with the polar constant, $m = 2$, is higher than that for an ellipse with eccentricity, $e = 0.9$. Hence, for an identical surface area, an equiangular spiral will have a lower value of 'a', and thereby, a lower value of the film thickness, too.

Fig. 6 depicts the variation of local Nusselt number along the length of the tube periphery for surfaces with different geometries at a given value of free stream concentration of the non-condensable species, $C_{g,\infty} = 0.1\%$. The decrease in local Nusselt number along the surface is attributed to the increase in liquid film thickness due to condensation. A comparison between the heat transfer performances of the tube with elliptic profile and that for an equiangular spiral reveals that the tube with spiral geometry facilitates greater heat transfer than that done by the ellipse. This may be attributed to the fact that the liquid film thickness for spiral geometry is lower than that for an elliptic tube, as established in Fig. 5. It is noteworthy to mention that the heat transfer performance for elliptic tubes increases marginally with an increase in ellipticity of the tube from 0 to 0.45, while there is a sudden increase in heat transfer rate with an increase in eccentricity from 0.45 to 0.9. This is in accordance with the results reported by Mosaad [9] for film condensation in absence of non-condensable species. This observation can be sensed from the plots of $F(\theta)$ vs. θ (Fig. 4) for an ellipse, where a sudden rise in $F(\theta)$ takes place with an increase in eccentricity from 0.6 to 0.9.

The most important feature of the present work is to evaluate the role of non-circular surface geometry as compared to a simple circular one in heat transfer augmentation capability to combat a drastic reduction in condensation heat transfer rate due to the presence of non-condensable species at free stream. Fig. 7 depicts this picture through a plot of $\frac{\overline{Nu_p}}{\overline{Nu_c}}$, as a function of the free stream concentration of the non-condensable species, $C_{g,\infty}$, for spiral and elliptic geometries of the tube surface. The subscripts 'p' and 'c' for Nusselt number, Nu, refer to non-circular and circular surface geometries, respectively. It is observed that the enhancement in heat transfer rate, with respect to a circular tube, is more for a spiral geometry than for an elliptic geometry. It is found that the enhancement for an ellipse of eccentricity, $e = 0.45$ is quite low, while it is substantially high for an ellipse of eccentricity, $e = 0.9$. For a spiral geometry, the value of $\frac{\overline{Nu_p}}{\overline{Nu_c}}$ steadily increases with an increase in polar constant 'm' of the surface. It is interesting to note that for both the polar and elliptic surfaces, the heat transfer enhancement is substantial with higher mass fraction of non-condensable gases present in the free stream.

4. Conclusions

A generalized mathematical model has been developed to determine the role of different non-circular horizontal tube surface geometries, namely, an equiangular spiral and an ellipse, as compared to a simple circular one, in heat transfer enhancement capability in laminar film condensation in presence of non-condensable gases. An air–water vapour system has been considered for demonstrating the mathematical model. The major conclusions drawn from the present study are as follows:

1. The liquid film thickness turns out to be lower in case of a surface with spiral geometry, as compared to that for an elliptic profile. The film thickness decreases with an increase in the concentration of non-condensable species present in the free stream.

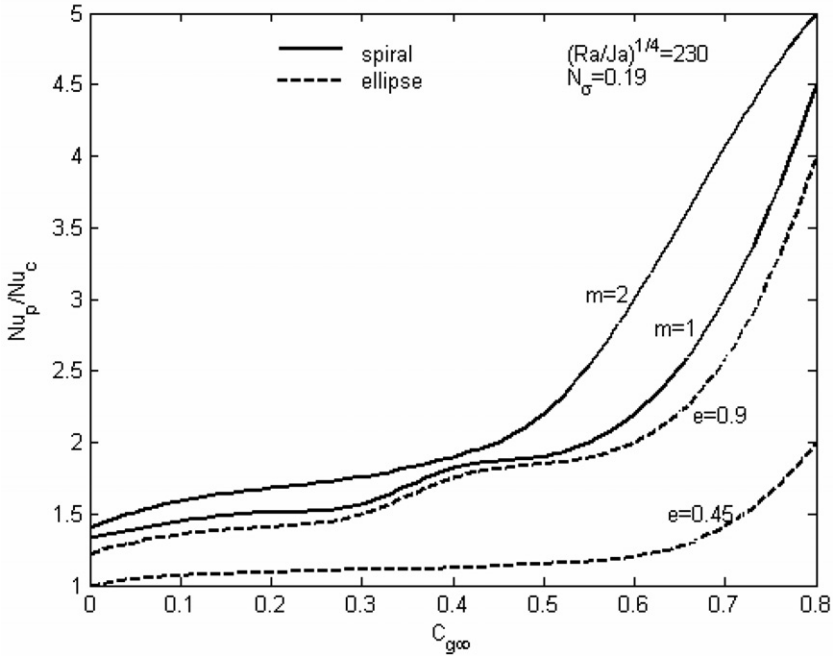

Fig. 7. Ratio of the averaged Nusselt number for the polar surfaces to that of an equivalent circular surface, for different values of free stream mass fraction of the non-condensable gases. The concentration values in the figure are represented in percentage units.

2. An enhancement in the overall heat transfer rate, for both elliptic and spiral surfaces, with respect to an equivalent circular tube surface, has been observed. This is attributed to the combined effect of gravity and surface tension driven favourable pressure gradient in the direction of condensate flow. The enhancement is more for a spiral surface as compared to that for an elliptic one. For an elliptic surface, there is a sharp increase in this enhanced rate of heat transfer when eccentricity, e increases from 0.45 to 0.9, and the similar trend takes place for a spiral surface when the polar constant, m changes from 1 to 2. The enhancement in heat transfer for non-circular tubes is more prominent at higher concentration of non-condensable gases present in the free stream. This suggests that tube surfaces with non-circular geometries can be utilized to a significant advantage, for maintaining substantial rates of condensation heat transfer even in the presence of non-condensable gases, provided that the manufacturing difficulties do not counterweigh this additional gain in heat transfer.

References

[1] W. Nusselt, Des Oberflachenkondensation des Wasserdamfes, Z. Vereines Deutsch. Ing. 60 (1916) 541–564, 569–575.

[2] S.S. Kutateladze, I.I. Gogonin, Heat transfer in condensation of flowing vapour on a single horizontal cylinder, Int. J. Heat Mass Transfer 28 (1985) 1019–1030.

[3] V. Dhir, J. Lienhard, Laminar film condensation on plane and axisymmetric bodies in non-uniform gravity, ASME J. Heat Transfer 93 (1971) 97–100.

[4] S. Cheng, J. Tao, Study of condensation heat transfer in elliptical pipes in a stationary saturated vapour, ASME J. Heat Transfer 96 (1988) 405–408.

[5] S. Yang, C. Chen, Laminar film condensation on a horizontal elliptical tube with variable wall temperature, Int. J. Heat Mass Transfer 116 (1994) 3135–3141.

[6] G.P. Fieg, Laminare Filmkondensation an geneeigten elliptischen Rohren unter dem Einfluss von Schwerkraft und Oberflaechenspannung, Fortschr.-Ber. VDI Reihe 19 Nr. 7. Duesseldorf: VDI-Verlag (1986) ISSN 0178-9465/ISBN 3-18-140719-4; G.P. Fieg and W. Roetzel, Calculation of laminar film condensation in/on inclined elliptical tubes, Int. J. Heat Mass Transfer 37 (1994) 619–624.

[7] S. Yang, C. Hsu, Mixed-convection laminar film condensation on a horizontal elliptical tube with uniform surface heat flux, Numer. Heat Transfer 32 (1997) 85–95.

[8] M. Asbik, D. Hadda, B. Zeghmati, A. Khmou, Forced convection laminar film condensation of downward flowing vapour on a single horizontal elliptical cylinder or a bank of elliptical tubes, Numer. Heat Transfer 37 (2000) 511–544.

[9] M. Mosaad, Mixed-convection laminar film condensation on an inclined elliptical tube, ASME J. Heat Transfer 123 (2001) 294–300.

[10] S.B. Memory, V.H. Adams, P.J. Marto, Free and forced convection laminar film condensation on horizontal elliptical tubes, Int. J. Heat Mass Transfer 40 (1997) 3395–3406.

[11] Sheng-an Yang, Cha'o-Kuang Chen, Role of surface tension and ellipticity in laminar film condensation on a horizontal elliptical tube, Int. J. Heat Mass Transfer 36 (1993) 3135–3141.

[12] A. Dutta, S.K. Som, P.K. Das, Film condensation of saturated vapour over horizontal non-circular tubes with progressively increasing radius of curvature drawn in the direction of gravity, ASME J. Heat Transfer 126 (2004) 906–914.

[13] E.M. Sparrow, E.R.G. Eckert, Effects of superheated vapour and non-condensable gases on laminar film condensation, AIChE J. 7 (1961) 473–477.

[14] E.M. Sparrow, S.H. Lin, Condensation heat transfer in the presence of a non-condensable gas, ASME J. Heat Transfer 86 (1964) 430–436.

[15] W.J. Minkowycz, E.M. Sparrow, Condensation heat transfer in the presence of non-condensables, interfacial resistance, superheating, variable properties, and diffusion, Int. J. Heat Mass Transfer 9 (1966) 1125–1144.

[16] D. Kroeger, W.M. Roshenow, Condensation heat transfer in the presence of non-condensable gas, Int. J. Heat Mass Transfer 9 (1973) 181–272.

[17] V.E. Denny, V.J. Jusionis, Effects of non-condensable gas and forced flow on laminar film condensation, Int. J. Heat Mass Transfer 15 (1972) 315–326.

[18] J.W. Rose, Condensation of a vapour in the presence of a non-condensing gas, Int. J. Heat Mass Transfer 12 (1969) 233–247.

[19] C.-Y. Wang, C.-J. Tu, Effects of non-condensable gas on laminar film condensation in a vertical tube, Int. J. Heat Mass Transfer 31 (1988) 2339–2345.

[20] A.C. Bannwart, A. Bontemps, Condensation of a vapour with in condensables: an improved gas phase film model accounting for the effect of mass transfer on film thickness, Int. J. Heat Mass Transfer 33 (1990) 1465–1474.

[21] T. Mamyoda, K. Asano, Experimental study of condensation of vapours in the presence of non-condensable gas on a short horizontal tube, Can. J. Chem. Eng. 27 (1994) 485–490.

[22] P.K. Sarma, M. Anjaneya Reddy, A. E Bergles, Sadik Kakac, Condensation of vapours on a fin in the presence of non-condensable gas, Int. J. Heat Mass Transfer 44 (2001) 3233–3240.

[23] S.K. Som, S. Chakraborty, Film condensation in presence of non-condensable gases over horizontal tubes with progressively increasing radius of curvature in the direction of gravity, Int. J. Heat Mass Transfer 49 (2006) 594–600.

[24] K. Stephan, Interface temperature and heat transfer in forced convection laminar film condensation of binary mixtures, Int. J. Heat Mass Transfer 49 (2006) 805–809.

[25] S. Oh, S.T. Revankar, Experimental and theoretical investigation of film condensation with non-condensable gas, Int. J. Heat Mass Transfer 49 (2006) 2523–2534.